Journal of Aeronautics, Astronautics and Aviation, Vol. 56, No. 1S, pp. 93 – 106 (2024)
DOI: https://doi.org/10.6125/JoAAA.202403_56(1S).02

Numerical Investigation of Heat Transfer Enhancement via Dimpled Target Surface Configuration and Jet Arrangement in Impingement Cooling

Muhammad Fitri Mohd Zulkeple [1], Abd Rahim Abu Talib [1, 2 *], Mohammad Yazdi Harmin [1], Syamimi Saadon [1], Muhammad Hanafi Azami [3], Talal Yusaf [4]

[1]*Aerodynamics, Heat Transfer & Propulsion (AHTP) Research Group, Department of Aerospace Engineering, Faculty of Engineering, Universiti Putra Malaysia, 43400 Serdang, Selangor, Malaysia*
[2]*Aerospace Malaysia Research Centre, Faculty of Engineering, Universiti Putra Malaysia, 43400 Serdang, Selangor, Malaysia*
[3]*Kulliyah of Engineering, International Islamic University Malaysia, P.O. Box 10, 50728 Kuala Lumpur, Malaysia*
[4]*School of Engineering and Technology, Central Queensland University, Qld, Australia*

ABSTRACT

This research employs numerical simulation to investigate the influence of dimple configurations on heat transfer. Specifically, it focuses on the 3x3 array of jets directed at a dimpled target surface. The study explores various jet pitches ($P = 3D_j$, $4D_j$ and $5D_j$) and distances between jets and the dimpled surface ($H = 3D_j$, $4D_j$ and $5D_j$). Additionally, dimple designs were altered while keeping their volume constant, resulting in elongated dimples. This investigation comprehensively examines flow patterns and heat transfer properties across Reynolds number (Re) range of 5,000 to 15,000. Increasing the H/D_j ratio from 4 to 5 enlarges entrainment vortices near the target surface due to reduced cross flow intensity between adjacent jets. Conversely, reducing the ratio to 3 intensifies crossflow, delaying cooling jet detachment and enhancing heat transfer. Evaluating the smallest jet-to-jet pitch ($P_x = 3D_j$) reveals enhanced heat transfer to the target surface, driven by increased coolant mass flow rate per unit area compared to larger jet pitches ($P_x = 4D_j$ and $P_x = 5D_j$). When altering dimple depths while maintaining constant volume, Nusselt numbers (Nu) showed improvements ranging from 10% to 16%, surpassing the 6% to 14% increase seen with hemisphere dimples.

Keywords: Heat transfer, Dimple, Impingement cooling, Jet arrangement, Numerical

I. INTRODUCTION

Scientists and researchers have consistently strived to improve the design and performance of aircraft and spacecraft. These ongoing efforts have led to innovations such as the adoption of alternative fuels in gas turbines, resulting in enhanced efficiency and reduced environmental effects [1,2]. Additionally, advancements in satellite structural technology have been made to boost reliability and extend their operational lifespan [3,4]. These breakthroughs are ushering the aerospace industry into an era filled with promising opportunities.

The use of jet impingement has become increasingly common in practical applications due to its superior heat transfer efficiency compared to alternative cooling methods, especially in energy systems like gas turbine engines [5]. Engineers have improved engine design by increasing compressor pressure ratios and turbine intake temperatures to enhance fuel conversion efficiency. However, these advancements have led to higher temperatures, necessitating effective cooling methods to

Manuscript received, September 26, 2023, final revision, October 17, 2023
* To whom correspondence should be addressed, E-mail: abdrahim@upm.edu.my

prevent component failure. Jet impingement, a forced convection method, shows promise in addressing this challenge and complying with emissions regulations.

The use of jet impingement has become increasingly common in practical applications due to its superior heat transfer efficiency compared to alternative cooling methods, especially in energy systems like gas turbine engines [5]. Engineers have improved engine design by increasing compressor pressure ratios and turbine intake temperatures to enhance fuel conversion efficiency. However, these advancements have led to higher temperatures, necessitating effective cooling methods to prevent component failure. Jet impingement, a forced convection method, shows promise in addressing this challenge and complying with emissions regulations.

Previous research extensively studied single [6] and multiple jet configurations [7-10], revealing variations in thermal characteristics due to interactions among adjacent jets a shown in Figure 1. Multiple jets offer advantages by achieving higher heat transfer coefficients and minimizing surface non-uniformities, crucial for cooling and heating applications. Surface alterations such as dimples have been explored and they show enhanced heat transmission, especially in concave dimples [11].

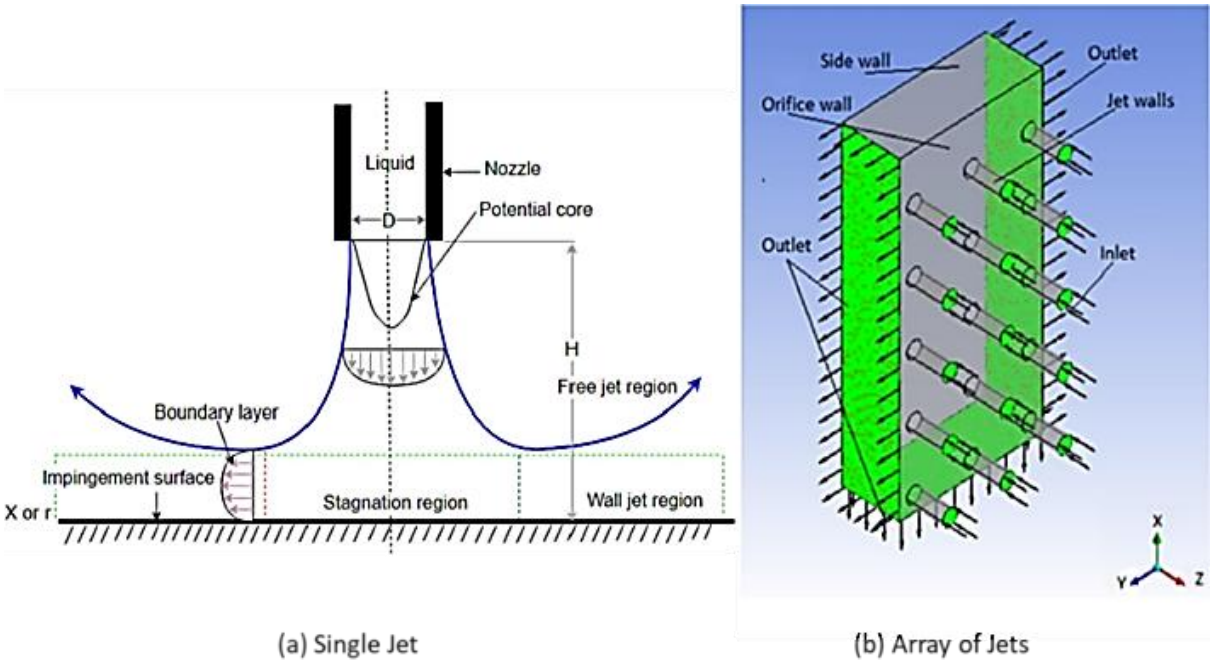

Figure 1 Hole configuration (adapted from [10] and [6], respectively)

Changing surface properties also contributes to improving heat transfer performance. In a prior study by Azad et al. [12], the researchers conducted experiments to understand the behavior of *Nu* on dimple surfaces. They found that *Nu* for hemispherical dimples, arranged in two distinct patterns, closely resembled those of a smooth surface within the *Re* range of 4,850 to 18,300. This enhanced heat transmission on dimpled surfaces is primarily attributed to their larger surface area. However, Ekkad and Kontrovitz [13] discovered a positive correlation between crossflow and heat transfer within the *Re* range of 4,800 to 14,800, indicating improved heat transfer coefficients in the presence of concave dimples.

Kanokjaruvijit et al., [14-18] conducted an extensive experimental study covering various factors, including Reynolds number (Re = 5,000 – 11,500), jet-to-plate spacing (z/d = 2, 4, 8, and 12), dimple depth (t/d = 0.15, 0.25, and 0.29), and the ratio of jet to dimple diameter (d/D_d = 0.25, 0.5, and 1.15) which was summarized in Table 1. They explored surface characteristics of cusped elliptical dimples alongside hemispherical ones and concluded that dimpled surfaces generated more vigorous vortices, enhancing heat transfer efficiency compared to both flat plates and cusped elliptical dimples.

The study conducted by Xing and Weigand [19] investigated the impact of a jet array on both flat and dimpled plates within a *Re* range of 15,000 to 35,000. They focused on the ratio of the spacing between the jet and plate (z) to the jet diameter (d), varying from 3 to 5. Optimal heat transfer performance was achieved by minimizing crossflow and maintaining a short distance between the jet and the plate, regardless of the plate's flatness or dimples. Dimples on the target plate enhanced heat transfer, especially under conditions of maximum and minimum crossflow. The crossflow approach yielding the lowest heat transfer performance was considered the most optimal, regardless of surface type. However, it was noted that dimpled surfaces performed better with increasing crossflow conditions.

Table 1 Summarized work done by Kanokjaruvijit et al., [14-18]

Reference	Design Parameter	Finding
[14][15]	Jet Hole $D_j = 0.59\ D_d$ $Pitch = 40\ mm$ $Re\ =\ 11000\ \&\ 11500$ Dimple $D_d = 17.32\ mm\ (Hemisphere)$ $D_d =\ 14.5\ mm\ (Cusp)$ $Dimple\ Depth, d\ =\ 5\ mm$ $Dimple\ Pitch\ =\ 40\ mm$ Jet to target Distance $\frac{H}{D_j} =\ 2, 4\ \&\ 8$	• H/D of 2 reduced heat transferred of both dimple geometries relative to the flat plate, presumably due to aggressive recirculation. • They performed similarly with the same equivalent dimension or cross-sectional area of hemispherical and cusped elliptical dimples. • The dimple-aligned jet holes had stronger effects than the flat ones. Some spent air flew into the dimples, losing momentum after impact. The heat transfer enhancement was lower than when jets hit dimples.
[16]	Phase 1 $D_d = 1.73D_{\ j}$ $Re = 5000, 8000, 11500$ $d = 0.25\ D_d$ $H = 2D_j, 4D_j, 8D_j, 12D_j$ Phase 2 $D_d = 2.0\ D_j$ $Re = 5000, 8000, 11500$ $d = 0.15D_d, 0.25D_d$ $H = 1D_j, 2D_j, 4D_j, 8D_j, 12D_j$	• High Reynolds number flow had more energetic eddies. Dimples broke down those eddies into smaller pieces, improving heat transfer, as seen by $Re = 11500$ and $H/Dj = 8$, where heat transfer was 50% better than the flat plate. • Narrow spacing might create recirculation and reduce heat transfer. At wide spacing, enhancement was lower. However, following shallower dimple experiments show significant heat transfer enhancement for narrow spacing. • Same-wetted-area hemispherical and cusped elliptical dimpled shapes were created. However, the cusp divided the approaching jet into two halves, creating stronger recirculation than the hemispherical dimple and reducing heat transfer. • Shallower dimples ($d/Dd = 0.15$) increase heat transfer more than deeper ones ($d/Dd = 0.25$) because vortices can be shed more easily. Recirculation rolling-up for shallow dimples may be harder.
[17]	**Phase 1** $D_d = 17.32\ mm$ $D_j = 10\ mm$ $Re = 11500$ $H = 2D_j, 4D_j, 8D_j, 12D_j$ $d = 0.29D_d$ **Phase 2** $D_d = 40\ mm$ $D_j = 20\ mm$ $Re = 5000, 8000, 11500$ $H = 1D_j, 2D_j, 4D_j, 8D_j, 12D_j$ $d = 0.15D_d, 0.25D_d$ **Phase 3** $D_d = 40\ mm$ $D_j = 10\ mm$ $Re = 11500$ $H = 2D_j, 4D_j$ $d = 0.15D_d, 0.25D_d$ **Phase 4** $D_d = 17.32\ mm$ $D_j = 20\ mm$ $Re = 11500$ $H = 2D_j, 4D_j$ $d = 0.29D_d$	• The hemispherical dimples increased heat transfer. Because two hemispherical dimples formed a cusped elliptical dimple, more recirculation was supposed to occur. • Impinging on flat areas increased heat transfer for shallow dimples, but vice versa for deep dimples. This was likely because shallow dimples shed vortices better and jets lost more momentum in deep dimples. • Raising jet exit velocity increased jet momentum at stagnation zones, boosting heat transfer. • Narrow H/Dj values (< 2) generated strong dimple recirculation and heat transfer deterioration compared to the flat plate. However, $H/Dj > 8$ spacing caused jets to lose velocity to ambient air and the transfer of heat to decrease. • Shallow dimples improved heat transfer more than deep ones because they created less recirculation and shed vortices faster. Shallow dimples also increased downstream surface static pressure. • Small $Dj\ /Dd$ values like 0.25 impinged totally inside the dimples. After impinging, the jets lost a lot of momentum inside the dimples, so the crossflow was too weak to detach and restart the boundary layer. More dimples were covered by the stagnation zone at $Dj\ /Dd = 1.15$. More edges detached from the border layer, and more high heat transfer zones were identified compared with previous $Dj\ /Dd$ values.

[18]	$D_d = 17.32\ mm, 40\ mm$ $D_j = 0.25D_d, 0.5D_d, 1.15D_d$ $Re = 5000, 8000, 11500$ $H = 1D_j, 2D_j, 4D_j, 8D_j, 12D_j$ $d = 0.15D_d, 0.25D_d, 0.29D_d$	• Increasing Re, will means am increases of jet exit velocity, which increases jet momentum at stagnation zones and heat transfer. • Narrow H/Dj values (< 2) resulted in extensive recirculation from the dimple and reduced heat transfer relative to the flat plate. Wider spacing like $H/Dj > 8$ caused jets to lose velocity to ambient air and reduce heat transmission. • The Nusselt number of heat transfer of dimple impingement was connected to dimensionless parameters like Reynolds number (Re), jet-to-plate spacing (H/Dj), dimple depth (d/Dd), and curvature. i. For impinging on dimples; $\overline{Nu}_{on\ dimples} = 0.1770\ Re^{0.61} \left(\frac{H}{D_j}\right)^{-0.23} \left(\frac{d}{D_d}\right)^{-0.60} \left(\frac{D_j}{D_d}\right)^{0.85}$ ii. For impinging on flat portion $\overline{Nu}_{on\ flat} = 0.3472\ Re^{0.5} \left(\frac{H}{D_j}\right)^{-0.16} \left(\frac{d}{D_d}\right)^{-0.64} \left(\frac{D_j}{D_d}\right)^{0.31}$

Numerical investigations, as demonstrated by studies from Kim and Kim [20] and Xie et al. [21], highlighted flow and pressure distribution across various flow configurations on dimpled surfaces. These studies revealed a positive correlation between dimple depth and the average increase in heat transfer. Nonetheless, Luo et al. [22] conducted a computational study that showed a thinning of the boundary layer and increased heat transfer near the edges of dimples with the presence of dimples. However, as dimple depths increased, heat transfer decreased.

Two separate studies by Schukin et al. [23] and Chang et al. [24] examined the impact of hemispherical cavities with concave and convex dimples, respectively, on convective heat transfer. The findings indicated that concave dimples outperformed a smooth surface in convective heat transfer. However, the *Nu* over the convex-dimpled surface was nearly twice that of a smooth surface, significantly affecting heat transport over the inter-jet zones. Chang and Liou [25] further investigated the impact of an impinging jet-array on both concave and convex dimpled surfaces, concluding that while concave dimples tended to have lower *Nu* compared to their convex counterparts, this was likely due to the development of recirculating flows within concave dimples. As Reynolds numbers increased, the ratios of Nusselt number (*Nu*) to Nusselt number for a smooth wall ($Nu_{\text{smooth-wall}}$) gradually fell over the dimpled surfaces, indicating diminishing heat transfer improvement.

Additionally, Huang and colleagues [26] conducted numerical investigations exploring the effects of various impinging jet and dimpled surface configurations on heat transfer enhancement. Their experimental findings showed that convex dimpled surfaces exhibited superior heat transmission performance compared to flat, concave, and mixed dimpled surfaces. The presentation of numerical findings and analysis of flow distribution across convex and concave dimpled surfaces significantly contributed to understanding fluid dynamics over such surfaces.

In a study by Singh and Ekkad [27], they explored the effects of repeated jet impingement on both dimpled and smooth surfaces subjected to rotation. While a smooth surface showed enhanced heat transfer, particularly in leading and trailing sections, rotation had an adverse effect on heat transport when considering a dimpled surface.

In a separate study, Vinze et al. [28] examined multiple jets emanating from orifices arranged in a 3x3 array. The investigation spanned a range of *Re* from 5,000 to 40,000, exploring various dimple and orifice pitches, dimple depths, eccentricity between the orifice and dimple, and spatial separation between the orifice plate and test surface. The experimental findings indicated that, for specific nozzle diameters where the pitch was three times the diameter, the flat plate was more efficient compared to dimpled surfaces. However, dimpled surfaces exhibited superior performance with higher pitches ($p \geq 4d$), especially with shallow dimples ($t/d = 0.25$) and a pitch of $5d$. The coefficient of variation (COV) suggested a more uniform distribution of *Nu* when the pitch equaled $3d$.

In summary, extensive research has been conducted on the influence of dimples on heat transfer, but there's limited study on dimple shapes beyond hemispheres. This study aims to conduct a numerical analysis of hemispherical and hemi-cylindrical dimple shapes, jet spacing, and orifice-to-target surface spacing within a *Re* range of 5,000 to 15,000. The findings will enhance our understanding of heat transfer prediction with surface dimples and facilitate improved surface design for optimized heat transfer efficiency. In past decade, there were more and more contraries committed to develop and research on unmanned aerial system (UAS) and unmanned aerial vehicle (UAV). Most obvious features of UAV are low-cost, high-flexibility, high-automation and high-

resolution for detection. Based on previous causes, UAV gradually replaced manned aircraft to execute common mission including disaster relief, airborne support. As for special missions are landscape photography and military reconnaissance. Special UAV likes USA RQ-4 Global Hawk. Its endurance and flight range are over 24 hours and larger than 25,000 km. It can perform long-term military reconnaissance mission in the battle. In order to simulate flight trajectory of cruise missile and improve training efficiency, the Flamingo II UAV in Taiwan was developed to be a military drone aircraft. Until today, more and more different types UAV were used for different military or civilian purposes.

II. SETUP AND METHODOLOGY

2.1 Geometric Model

Figure 2 illustrates a 3-D model of multiple jet impingement. The rectangular channel features a symmetrical arrangement of three jet holes evenly distributed across three rows. The channel exhibits symmetry in both the X and Z directions. On the other hand, in Figure 3, the top view of the channel reveals that the diameter of the jet hole, referred to as D_j, measures 6 mm. Furthermore, the jet-to-jet spacing or pitching, represented by P_x and P_z, is determined to be $3D_j$, $4D_j$ and $5D_j$. The channel's dimensions, specifically its length (L) and width (W), are 140 mm and 100 mm, respectively.

Meanwhile, Figure 4 depicts the surfaces targeted by the representation. The heights of the jet holes and the main channel, denoted as H, are equal to $3D_j$, $4D_j$, and $5D_j$, respectively. The diameter of the dimples on the hemisphere, referred to as D_d, is established to be equal to the diameter of the jet hole, denoted as D_j. Additionally, the depth of the hemisphere, referred to as $t_{\text{hemisphere}}$, is set to half of the diameter D_d.

The dimensions of the hemi-cylindrical shape, also known as a trench or dimple, were determined by considering the volume of the hemisphere-shaped dimple. The depth, denoted as $t_{\text{hemicylindrical}}$, was varied between $0.4D_j$, $0.3D_j$ and $0.2D_d$. The length of the hemi-cylindrical dimple, l_{hc} can be defined by the following Equation (1).

$$l_{hc} = \frac{4}{3}\left(\frac{r_{hemisphere}^3}{t_{hemicylindrical}^2} - t_{hemicylindrical}\right) + 2t_{hemicylindrical} \quad (1)$$

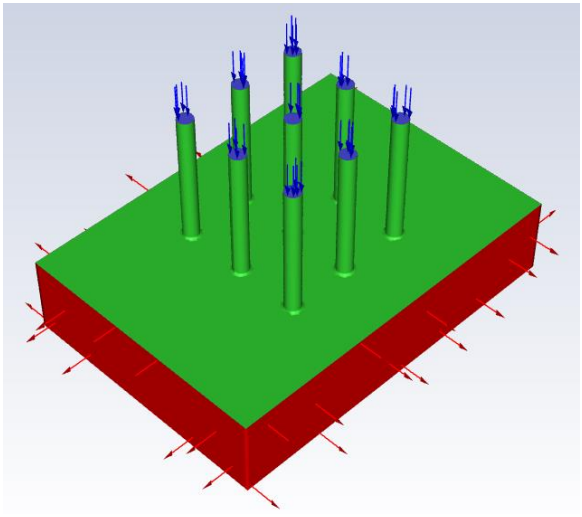

Figure 2 Computational model of CFD

It is assumed that the fluid flow at the beginning of the channel is fully developed and hydrodynamically stable. At the channel exit, all streamwise gradients for various properties are uniformly set to zero. The bottom wall of the model, which features a dimpled surface, is exposed to a uniform heat flux of 2 kW/m^2. The other walls and sections of the test area are adiabatic surfaces.

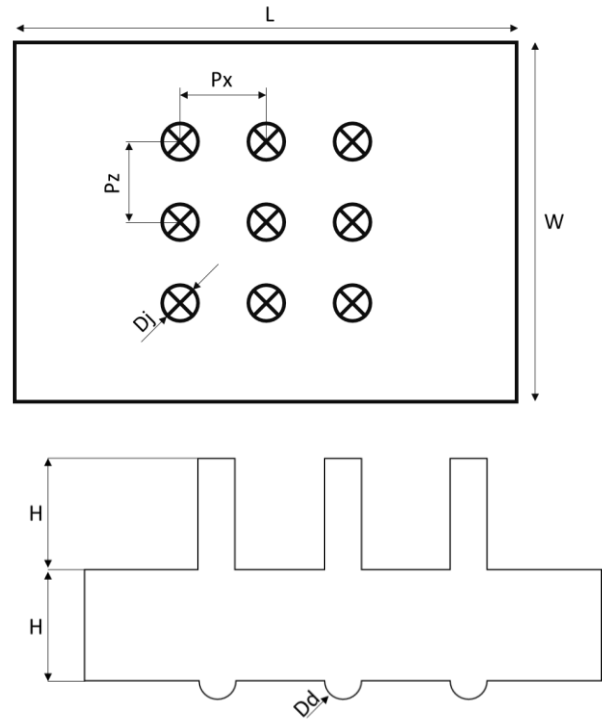

Figure 3 Top (left) and side (right) view of the model

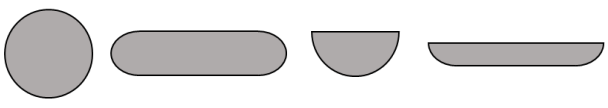

Figure 4 Representative dimple shape
(a) top view, (b) side view

2.2 Governing Equations

Numerical simulations were performed using the commercially available software Ansys FLUENT. These simulations were based on solving the Reynolds-averaged Navier-Stokes (RANS) equations coupled with turbulent model equations to obtain computational results. Specifically, the Shear Stress Transport (SST) turbulence model, as proposed by Metre [29], was employed in this investigation. The SST model was developed to address limitations observed in the *k*-ε and *k*-ω models. According to Culun et al. [10], the SST model is highly accurate in predicting flow separation, especially under adverse pressure gradients, as often encountered in impinging jet simulations. This accuracy is attributed to the model's incorporation of transport effects in calculating eddy viscosity, allowing for precise estimations of flow separation onset and magnitude.

The convergence of the simulation results was determined by monitoring the stability and magnitude of the root mean square residuals, which needed to remain constant and below a threshold of 1×10^{-6}. The SST model was formulated using the Reynolds-Averaged Navier-Stokes (RANS) equations for momentum and mass conservation. In this study, the turbulence model involved solving the *k*-ω model at the wall and the *k*-ε model in the bulk flow. To keep things straightforward, the RANS equations used in this study were expressed in Cartesian tensor form.

The continuity equation and the momentum equation are given by Equation (2) and Equation (3), respectively.

$$\frac{\partial}{\partial x_i}(\rho u_i) = 0 \tag{2}$$

$$\frac{\partial}{\partial x_i}(\rho u_i u_j) = -\frac{\partial p}{\partial x_i} + \frac{\partial}{\partial x_i}\left((\mu + \mu_t)\frac{\partial u_j}{\partial x_i}\right) \tag{3}$$

where $j = 1, 2, 3$

The SST turbulence model comprises of a pair of transport equations: one governing the turbulence kinetic energy κ and the other governing the particular rate of turbulence destruction ω. These are given by Equation (4) and Equation (5). Note that the SST equations involve several important variables. One of these variables is ω, which represents the specific rate at which turbulence is dissipated. Another variable, denoted as P_κ, indicates the rate at which turbulent kinetic energy κ is generated. Additionally, terms such as σ_κ, $\sigma_{\omega 1}$ and $\sigma_{\omega 2}$ are diffusion factors that govern the transport of κ and ω. The blending function F_1 plays a role in combining the standard *k*-ε model with the Wilcox *k*-ω model. Another fundamental term in this context is the absolute value of the shear strain rate, represented as *S*. Model constants like *A* and β are also significant components of the model.

$$\frac{\partial}{\partial x_i}(\rho\kappa u_i) = P_\kappa - \beta_1\rho\kappa\omega + \frac{\partial}{\partial x_i}\left[\left(\mu + \frac{\mu_t}{\sigma_\kappa}\right)\frac{\partial \kappa}{\partial x_i}\right] \tag{4}$$

$$\frac{\partial}{\partial x_i}(\rho\omega u_i) = A\rho S^2 - \beta_2\rho\omega^2 + \frac{\partial}{\partial x_i}\left[\left(\mu + \frac{\mu_t}{\sigma_{\omega 1}}\right)\frac{\partial \omega}{\partial x_i}\right] + 2(1 - F_1)\rho\frac{1}{\sigma_{\omega 2}\omega}\frac{\partial \kappa}{\partial x_i}\frac{\partial \omega}{\partial x_i} \tag{5}$$

The solution of Equation (4) and Equation (5) yields the values of κ and ω, which are then used to evaluate the turbulent viscosity μ_t from Equation (6). In this equation, F_2 is a function that limits the values of the turbulent viscosity in the near-wall region, *a* is a constant and *S* has already been defined in connection with Equation (5). Further details of the SST model can be found in Menter [29].

$$\mu_t = \frac{a\rho k}{\max(a\omega, SF_2)} \tag{6}$$

For the heat transfer problem, the appropriate energy equation is given by Equation (7). In this equation, *k* is the molecular thermal conductivity (a fluid property) and k_t is the turbulent thermal conductivity. If a turbulent, Prandtl number can be defined using Equation (8). The default value of 0.9 was used for Pr_t since from experimental data, Pr_t ranges from 0.7 to 0.9 depending on the Prandtl number of the fluid in question.

$$\rho c_p\left(u_i\frac{\partial T}{\partial x_i}\right) = \frac{\partial}{\partial x_i}\left((k + k_t)\frac{\partial T}{\partial x_i}\right) \tag{7}$$

$$Pr_t = \frac{C_p\mu_t}{k_t} \tag{8}$$

2.3 Parameter Definitions

For describing the flow field and heat transfer characteristic of the impingement cooling, the following parameters are defined. In the numerical calculation, the *Re* ranges from 5,000 to 15,000 with a step size of 5,000. The *Re* is defined as in Equation (9), where ρ is the fluid density, *u* is the fluid velocity, *d* is the jet diameter and μ is the dynamic viscosity coefficient of the fluid.

$$Re = \frac{\rho u d}{\mu} \tag{9}$$

Meanwhile, the dimensionless heat transfer number, namely *Nu*, is calculated from the extracted results. The *Nu* is found through Equation (10), where *h* is the heat transfer coefficient, *d* is hydraulic diameter of the jet hole and *k* is the thermal conductivity of air.

$$Nu = \frac{hd}{k} \tag{10}$$

The heat transfer coefficients exported from post-processing in FLUENT-Post is calculated using Equation (11), where *q* is the heat flux, and T_w and T_j represent the target wall-temperature and jet temperature respectively.

$$h = \frac{q}{T_w - T_j} \tag{11}$$

2.4 Meshing Strategy

A global hexahedral mesh is created, and a grid dependence investigation is conducted using an example with a hemisphere dimple target at a *Re* of 5,000. The grid number has been expanded from approximately 160,000 to 3.1 million. Figure 5 illustrates the comparison of the average *Nu* of the target surface. The average *Nu* is depicted using a bar chart while the relative error is represented by a point line graph. Figure 6 shows a one-quarter of the CFD domain being used.

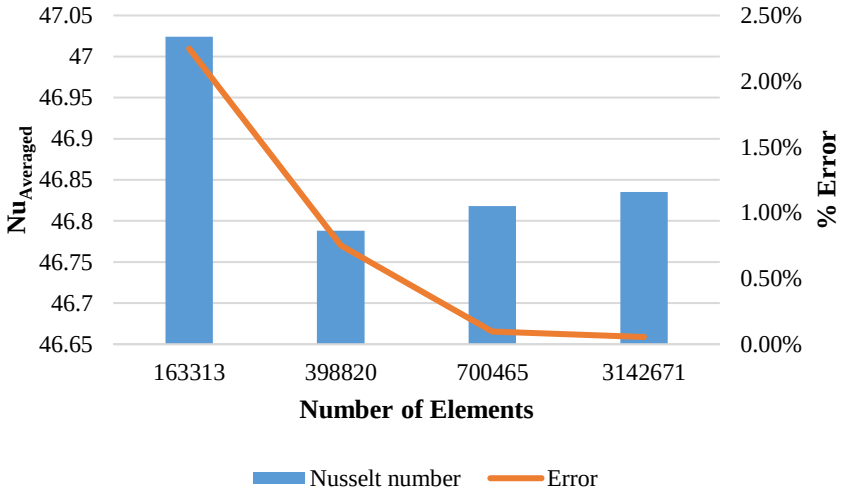

Figure 5 Mesh independency test

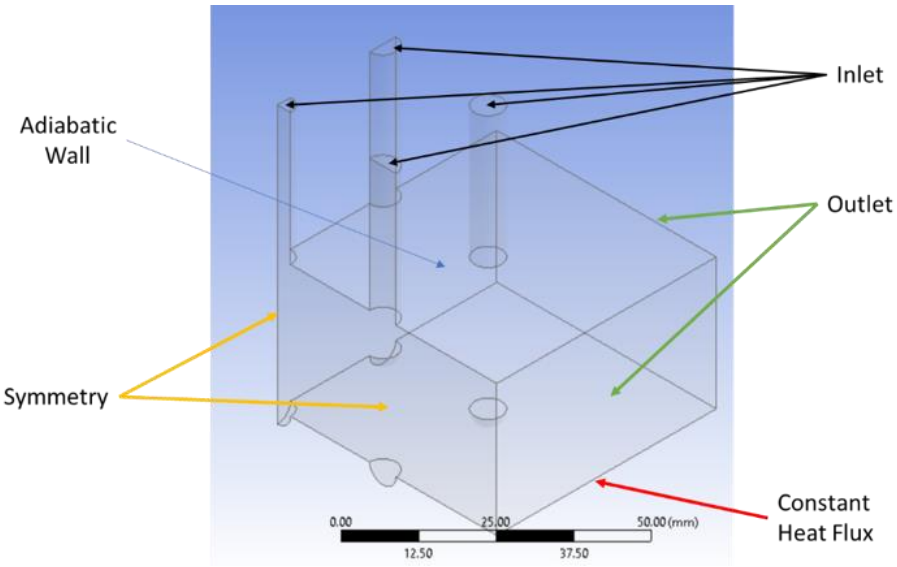

Figure 6 One-quarter of CFD domain

2.5 Boundary Conditions and Turbulence Model

The numerical model depicted in Figure 6 is designed to account for the flow channel's symmetry in both the *X* and *Z* directions, with a focus on computational efficiency. In this study, the working fluid is assumed to be ideal air at a temperature of 298 K and a pressure of 1 atm. At the inlet boundary, a uniform velocity is set, corresponding to a *Re* range of 5,000 to 35,000 with a turbulence intensity of 5%. The target surfaces are subjected to a constant heat flux of 2142 W/m^2. The two internal sides exhibit symmetrical characteristics and act as boundaries, while the remaining walls are considered adiabatic boundaries. Additionally, a no-slip boundary condition is applied to all walls except for the entrance and outflow.

The numerical computations in this study utilize the Reynolds-Averaged Navier-Stokes (RANS) approach and are carried out using the commercial software ANSYS-FLUENT. ANSYS-FLUENT provides a variety of turbulence models, and selecting the appropriate turbulence model is a critical aspect of these calculations. After reviewing the existing academic literature available in open databases related to impingement channels with three rows of nozzles, the experimental findings from

Vinze et al. [28], which involved multi-jet (9x9) impingement, were chosen as a reference.

Previous research suggests that the Shear Stress Transport (SST) turbulence model outperforms other models in accurately matching experimental results. The SST turbulence model has gained popularity for its ability to precisely simulate fluid flow and heat transfer. It combines the *k*-ε model in the central turbulence region and the *k*-ω model near the wall. Additionally, a study by Jing [30] supports the suitability of the SST model for assessing flow patterns and heat transfer over surfaces with dimples and protrusions. In this study, the SST turbulence model is employed.

The numerical calculations are considered converged as the residuals for continuity, momentum, energy equations, turbulence eddy frequency, turbulence kinetic energy, and wall temperature all fall below 10^{-6}. The wall temperature residual between consecutive iterations is also less than 1% as shown in previous Figure 5. To validate the simulation results, they are compared to the experimental data conducted by Vinze et al. [28], as presented in Figure 7.

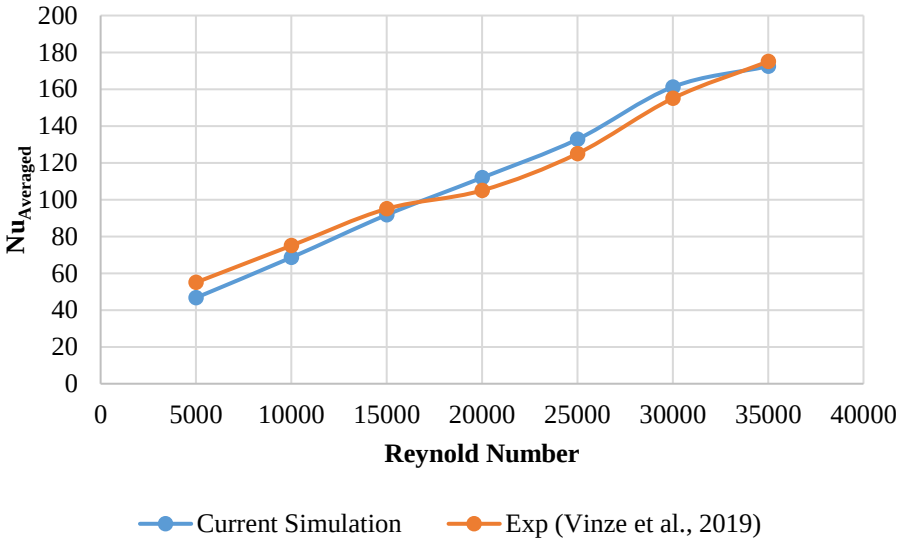

Figure 7 Simulation validation with Vinze et al. [28]

III. RESULTS AND DISCUSSION

3.1 Effects of Jet-to-Plate Spacing

The gap between the jet and the plate plays a crucial role in impingement cooling as it significantly impacts heat transfer characteristics and the spread of the flow field. Figure 8 illustrates how the heat transfer coefficient is distributed for various target spacings, where H/D_j values range from 3 to 5. As the H/D_j ratio increases, the distance between the jet and the impingement target surface also increases. Consequently, the area of high heat transfer coefficient on the target surface, corresponding to the impingement stagnation point, decreases rapidly. Moreover, the increased H/D_j ratio causes the incoming jet flow to deflect, making it less effective in impinging on the inner surface of the dimpled region. This deflection reduces the interaction among adjacent jets, leading to a decrease in heat transfer as shown visually in Figure 8(c).

Figure 9 illustrates a cross-sectional view along the streamwise direction of the dimensionless separation between the jet and the plate, H/D_j, with values of 3, 4 and 5. Upon observation, it becomes evident that as the gap between the jet and the plate is increased from 4 to 5, while maintaining a constant impingement *Re*, the intensity of crossflow between adjacent jets decreases. This decrease can be attributed to the expansion of the chamber's cross-sectional area. Consequently, the entrainment vortices near the target surface increase in size. As mentioned earlier, when the space between the jet and the plate widens, the incoming jet flow is redirected, resulting in improper entry into the dimple and limited contact with the dimple's edge. This causes the jet to rise higher above the intended surface upon exiting the dimple. As a result, the temperature differences between the high-temperature zone and the adjacent low-temperature stagnation zones become more significant.

Conversely, reducing the jet-to-target plate spacing H/D_j from 4 to 3 intensifies the crossflow within the impingement chamber due to the reduction in the flow area. The entering crossflow leads to increased suppression of entrainment vortices, causing a delay in the separation of the cooling jets from the impinging target wall. As time progresses, the temperature gradients along the surface decrease because of the reduced temperature differences between the high-temperature zone and the adjacent regions where the flow stagnates upon impingement.

Figure 10 presents the average *Nu* as a function of various *Re*, considering different dimensionless spacings between the jet and the target, represented as H/D_j, with values of 3, 4 and 5. The data illustrates that there is an

improvement in the average Nusselt number of the target plate as the Re increases. This correlation is more noticeable for H/D_j values of 3 when compared to values of 4 and 5. However, it is important to note that increasing the spacing doesn't always lead to unfavorable results. When the *Re* was raised to 10,000, the jet-to-plate spacing of 5 resulted in a higher average *Nu* compared to the case with a spacing ratio (H/D_j) of 4. This trend became even more evident when the *Re* was further increased to 15,000.

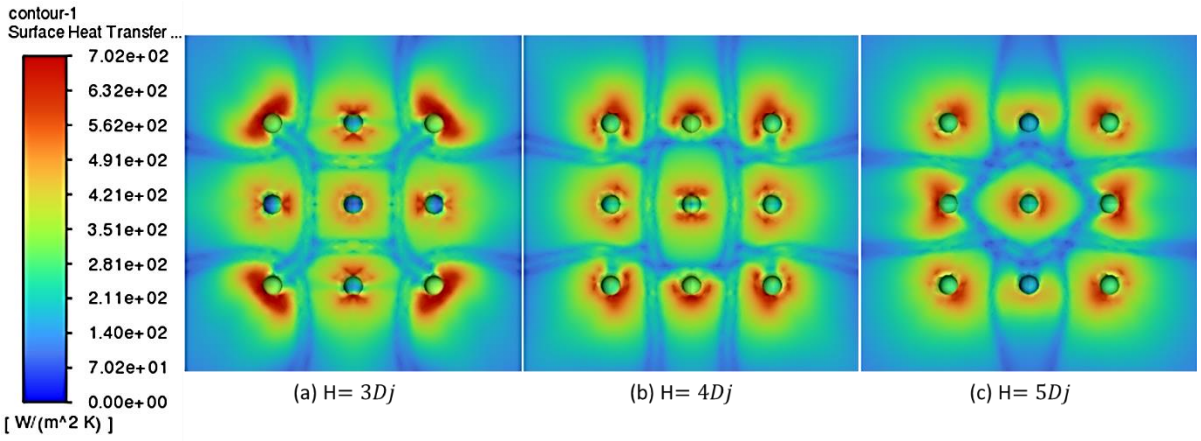

Figure 8 The target spacing heat transfer coefficient distribution, with H/D_j values from 3 to 5

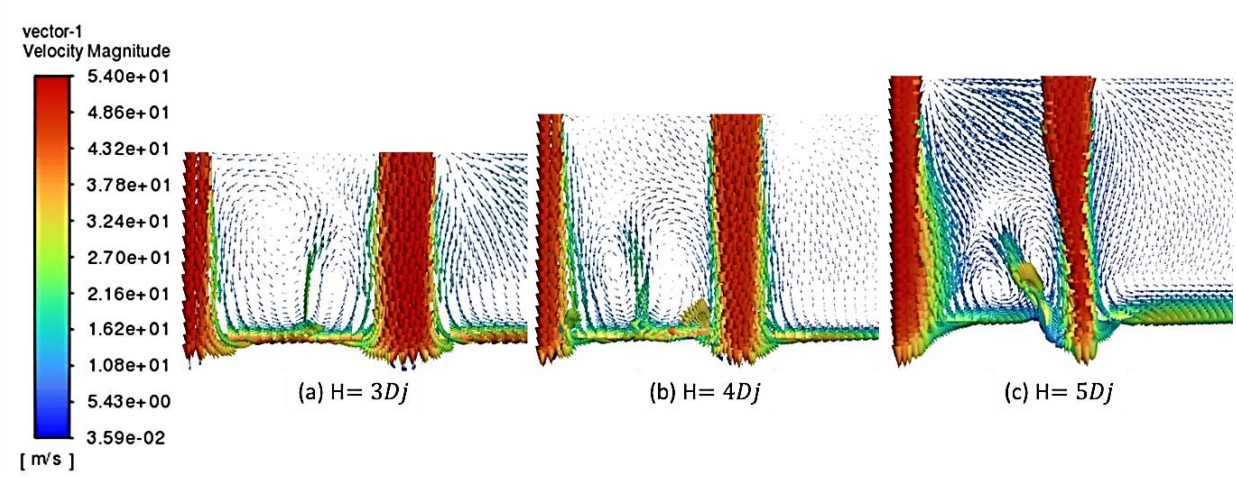

Figure 9 Dimensionless jet-to-plate spacing, H/D_j streamwise section

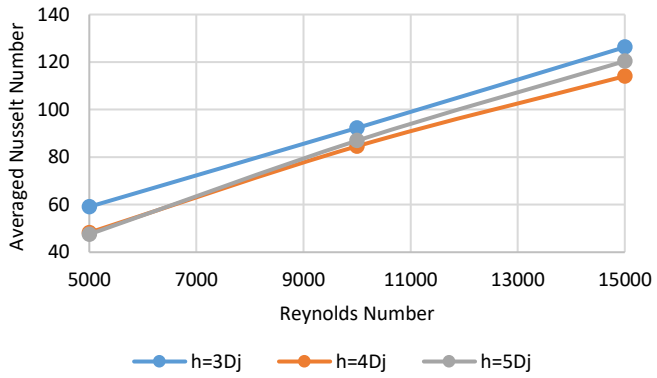

Figure 10 Average *Nu* as a function of *Re* and *H/D*

This phenomenon occurs because of the significant enhancement of inter-jet interaction and crossflow effects in situations with reduced distance. In cases of moderate jet flow rates, the momentum of the incoming fresh jet is dissipated by the crossflow of the exhaust gases. This leads to a reduction in heat transfer from the target plate.

3.2 Effects of Jet-to-Jet Pitch

Figure 11 demonstrates how the jet-to-jet spacing (P_x) affects heat transfer. It's noticeable that as the spacing between the orifice and jet increases, there is a corresponding decrease in the average heat transfer. When the three pitch configurations ($3D_j$, $4D_j$ and $5D_j$) are compared, it can be seen that, at a specific jet *Re*, the $3D_j$ pitch configuration provides a larger amount of coolant per unit area. This results in improved overall heat transfer to the designated surface. Figure 12 presents a plot that shows how variations in jet-to-jet pitches affect the *Nu*. When examining Figure 12, it is evident that the smallest jet-to-jet pitch ($P_x = 3D_j$) has a different *Nu* distribution along the streamwise direction compared to the higher jet-to-jet pitches ($Px=4Dj$ and $P_x=5D_j$). The distinctions are particularly noticeable in the confined area, where peaks emerge between adjacent jets. In the case of the shortest jet-to-jet pitch ($Px=3D_j$), the presence of a prominent peak between the jets indicates significant interference from nearby jets. However, as the distance between the jets increases, the peak begins to split in the center, indicating a decrease in jet interaction until they separate into two distinct peaks with less interaction, like what happens at a pitch of 5 times the jet diameter. Figure 13 provides a clearer view of these differences. With a pitch of $3D_j$, intense vortices form between the jets. Conversely, with a pitch of $5Dj$, the vortices occur at a lower level.

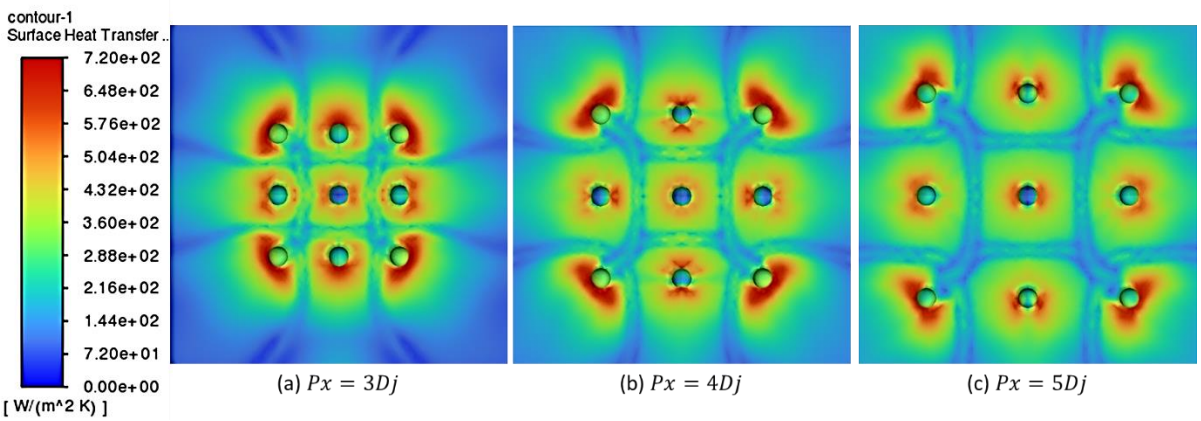

Figure 11 The heat transfer effect of jet-to-jet pitching (P_x)

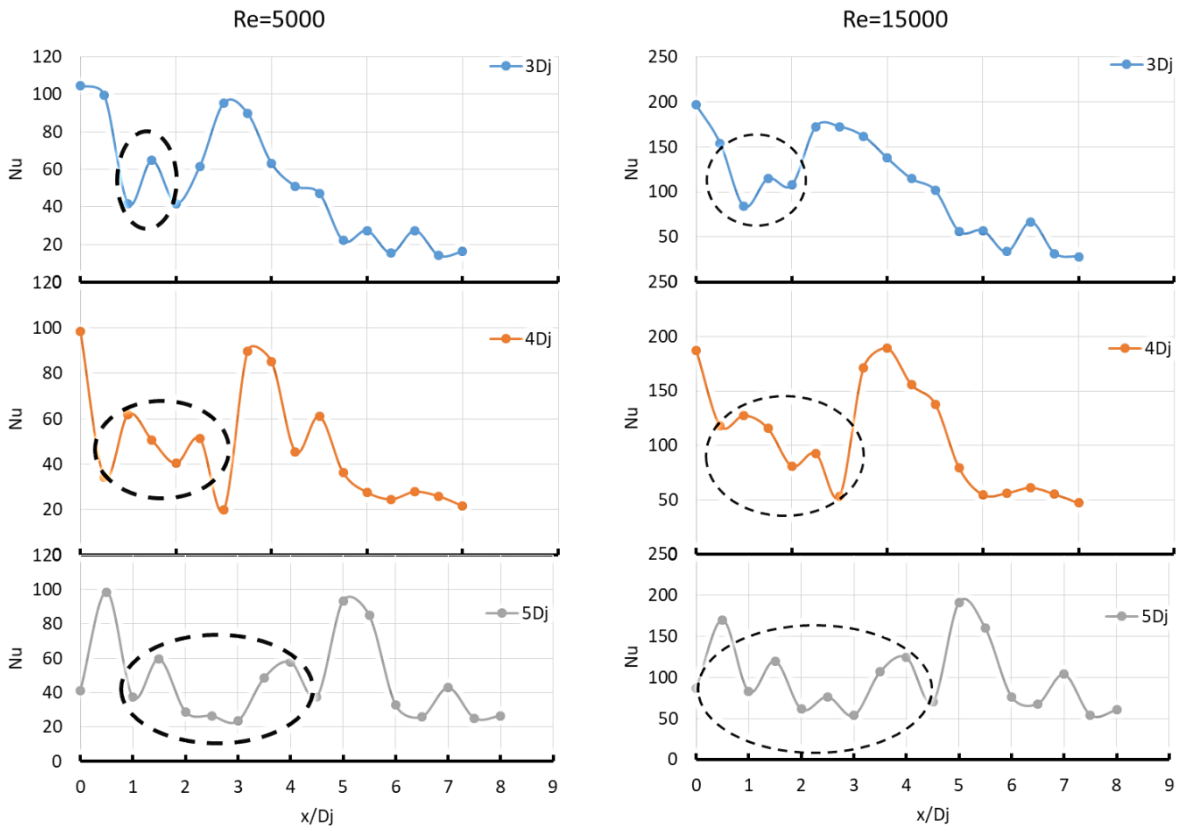

Figure 12 Variations in jet pitches affect *Nu*

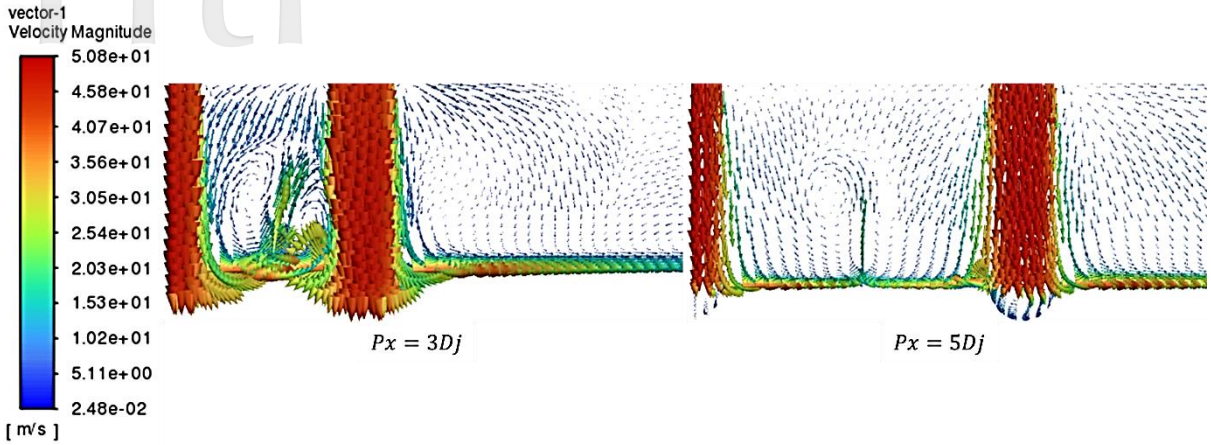

Figure 13 Jet-to-jet pitch, P_x streamwise section

According to some literature, the amount of air used to impact the target is influenced by both the number of impinging jets and the impingement *Re*. Therefore, it's not suitable to solely compare the heat transfer performances of different jet-to-jet pitches based on the jet *Re* [28]. However, studying this parameter is essential to comprehend how the spacing between the jets can affect the flow dynamics and thermal performance.

Based on the data presented in Figure 14, it is clear that there is a consistent upward trend observed across all examined jet-to-jet pitch values as the *Re* increases. With higher *Re*, there is an increase in the intensity and aggressiveness of flow interaction between the jets, leading to improved average heat transfer to the target surface. However, it's important to note that in the case of hemispherical dimpled surfaces, the presence of eddies within the dimples creates more resistance to the incoming coolant flow. As a result, some of the coolant doesn't reach the intended surface and instead gets lost in the strong cross flow. Therefore, it's evident that the heat transfer characteristics of a hemispherical dimpled surface are not significantly affected by the jet pitch and the dimpled plate design.

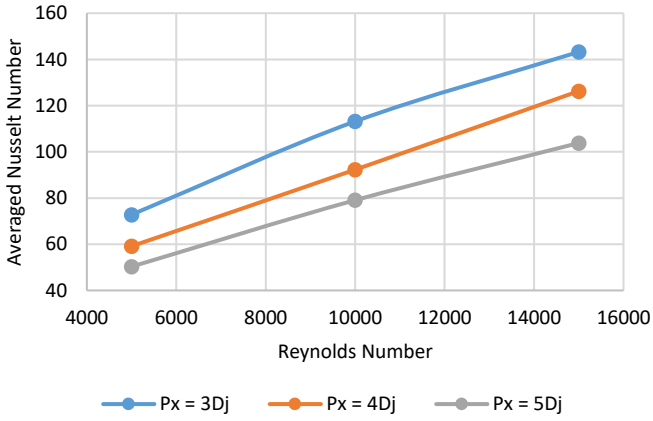

Figure 14 Reynolds numbers and jet-to-jet pitch affect the average *Nu*

3.3 Effects of Dimple Shape

Modifying the geometric features of the dimple has the potential to enhance heat transfer efficiency. Typically, dimples have a hemispherical shape or a similar form. As mentioned earlier, the presence of vortices within hemispherical dimples creates increased resistance to the incoming flow of fresh coolant. Consequently, some of the coolant doesn't reach its intended surface and instead disperses in the turbulent cross flow. Improvements in this aspect can be achieved by altering the geometric characteristics of the dimples. In this study, modifications were made to the dimple geometry while keeping the dimple volume constant. Specifically, the dimple depth was manipulated, varying it as 0.4 times the jet diameter ($0.4D_j$), 0.3 times the jet diameter ($0.3D_j$) and 0.2 times the jet diameter ($0.2D_j$). This manipulation resulted in elongating the dimple in the spanwise direction, effectively transforming it into a hemi-cylindrical shape.

The results presented in Figure 15 indicate that elongating the dimple in the spanwise direction led to an increase in the average *Nu*. More specifically, for dimples with depths of $0.4D_j$ and $0.3D_j$, enhancements ranging from 10% to 15% and 13% to 16%, respectively, were observed for *Re* ranging from 5,000 to 15,000 when compared to a smooth target surface. The presence of a typical hemispherical dimple was observed to result in an

enhancement ranging from 6% to 14% compared to a smooth target surface. This observation suggests that the existence of eddies within the dimples leads to increased resistance to the incoming flow of fresh coolant, which was mitigated when the dimple was elongated in a spanwise manner.

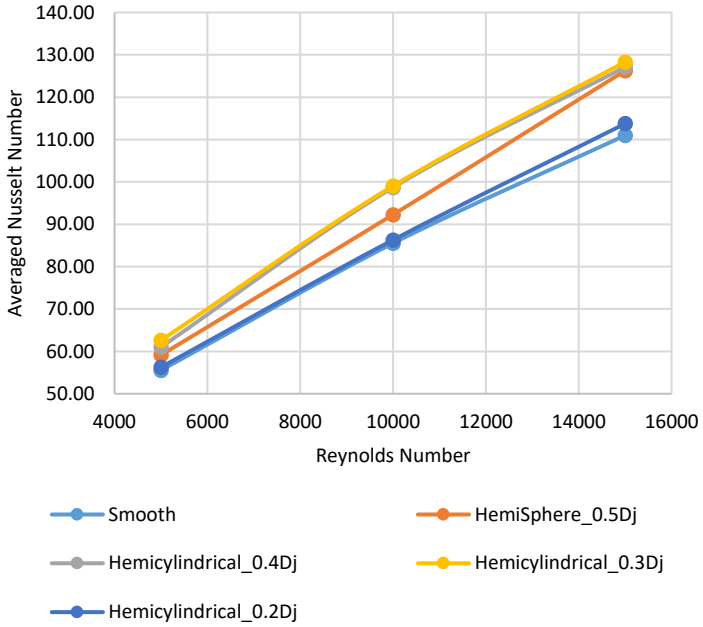

Figure 15 *Re* and dimple design affect average *Nu*

However, when the dimple depth was reduced to 0.2 times the diameter of the jet ($0.2D_j$), it was observed that the *Nu* remained within the same range as that of the smooth target surface. This suggests that while the jet effectively impacted the desired area with little eddy generation, the resulting depth may be too shallow to produce a noticeable difference in heat transfer compared to the smooth target surface when using the *Nu* as the measure.

IV. CONCLUSIONS

A numerical investigation was conducted to explore the heat transfer characteristics of a multiple jet array impingement cooling system across a range of *Re*, spanning from 5,000 to 15,000. This study delved into the effects of an array of jets with varying pitches (P_x=3D_j, 4D_j, and 5D_j) on a dimpled surface with different jet-to-plate spacings (H=3D_j, 4D_j, and 5D_j). The investigation encompassed the assessment of thermal performance, as measured by the Nusselt number, and the visualization of fluid dynamics, particularly the intensity of vortices. The findings of this analysis lead to the following conclusions:

- When the distance between the jet and the plate is extended from 4 to 5 while keeping the impingement *Re* constant, the intensity of crossflow between neighboring jets decreases. Consequently, the entrainment vortices close to the target surface grow. Conversely, reducing the spacing between the jet and the target plate (H/D_j) from 4 to 3 intensifies the crossflow within the impingement chamber. This is attributed to the reduction in available flow area. The entrainment vortices experience increased suppression due to the incoming crossflow, resulting in a prolonged delay before the cooling jet separates from the target wall upon impact.
- When considering the smallest jet-to-jet pitch (P_x=3Dj), it is evident that the *Nu* distribution along the streamwise direction exhibits a distinct trend compared to larger jet-to-jet pitches, specifically P_x=4D_j and P_x=5D_j. At a given *Re* for a jet, the 3D_j pitch configuration demonstrates a higher coolant mass flow rate per unit area. This leads to an increased rate of heat transfer to the specified surface.
- Altering the depths of the dimples while keeping the volume constant resulted in observed enhancements in the *Nu* ranging from 10% to 16%. In comparison, the typical hemisphere dimple exhibited enhancements ranging from 6% to 14% when compared to a smooth target surface. This observation suggests that the presence of eddies within the dimples increases resistance to the incoming coolant flow, which was mitigated by elongating the dimple in a spanwise direction.

ACKNOWLEDGMENTS

The authors would like to thank the Ministry of Higher Education (MoHE) for the funding allocated in this project under the Malaysia Spain Innovation Programme (MySIP) no. 5540547.

REFERENCES

[1] Rafiul Alam JA, Abu Talib AR, Altarazi YSM, Yusaf T, Azami MH, Nik Mohd NAR, "Experimental investigation on gas turbine engine performance using alternative fuel," *Journal of Aeronautics, Astronautics and Aviation*, Vol. 55, No. 3S, 2023, pp. 479-483.

[2] Alterazi YSM, Abu Talib AR, Yu J, Gires E, Abdul Ghafir MF, Lucas J, Yusaf T, "Simulating aero-engine performance and emissions characteristics running on green diesel," *International Journal of Green Energy*, Vol. 20, No. 4, 2023, pp. 372-377.

[3] Dawood SDS, Harmin MY, Harithuddin ASM, Ciang CC, Rafie ASM, "Computational study of mass reduction of a conceptual microsatellite structural subassembly utilizing metal perforations," *Journal of Aeronautics, Astronautics and Aviation*, Vol. 53, No. 1, 2021, pp. 57-66.

[4] Dawood SDS, Harithuddin ASM, Harmin MY, "Modal analysis of conceptual microsatellite design employing perforated structural components for mass reduction," *Aerospace*, Vol. 9, No. 1, 2022, 23.

[5] Dewan A, Dutta R, Srinivasan B, "Recent trends in computation of turbulent jet impingement heat transfer," *Heat Transfer Engineering*, Vol. 33, No. 4-5, 2012, pp. 447-460.

[6] Han B, Goldstein RJ, "Jet-impingement heat transfer in gas turbine systems," *Annals of the New York Academy of Sciences*, Vol. 934, No. 1, 2006, pp. 147-161.

[7] Ramli MS, Abu Talib AR, Harmin MY, Mohd. Saiah HR, "Effect of multiple jet impingement plate configurations on Reynolds number in a pipe", *IOP Conference Series: Materials Science and Engineering*, Vol. 152, 2016, 012012.

[8] Zulkeple MFM, Talib ARA, Gires E, Sultan MH, Ramli M, "Heat transfer performance of multiple holes impingement cooling technique," *International Journal of Engineering*, Vol. 7, No. 4, 2018, pp. 43-52.

[9] Shukla AK, Dewan A, "Flow and thermal characteristics of jet impingement: comprehensive review," *International Journal of Heat and Technology*, Vol. 35, No. 1, 2017, pp. 153-166.

[10] Culun P, Celik N, Pihtili K, "Effects of design parameters on a multi jet impinging heat transfer," *Alexandria Engineering Journal*, Vol. 57, No. 4, 2018, pp. 4255-4266.

[11] Florschuetz L, Metzger D, Takeuchi D, Berry R, "Multiple jet impingement heat transfer characteristics - experimental investigation of inline and staggered arrays with crossflow," NASA-CR-3217, Tempe, USA, 1980.

[12] Azad GS, Huang Y, Han JC, "Impingement heat transfer on dimpled surfaces using a transient liquid crystal technique," *Journal of Thermophysics and Heat Transfer*, Vol. 14, No. 2, 2000, pp. 186-193.

[13] Ekkad SV, Kontrovitz D, "Jet impingement heat transfer on dimpled target surfaces," *International Journal of Heat and Fluid Flow*, Vol. 23, No. 1, 2002, pp. 22-28.

[14] Kanokjaruvijit K, Martinez-Botas RF, "An experimental investigation of the heat transfer due to multiple jets impinging normally on a dimpled surface," *Proceedings of the Institution of Mechanical Engineers, Part C: Journal of Mechanical Engineering Science*, Vol. 218, No. 1, 2004, pp. 1337-1347.

[15] Kanokjaruvijit K, Martinez-Botas RF, "Jet impingement on a dimpled surface with different crossflow schemes," *International Journal of Heat and Mass Transfer*, Vol. 48, No. 1, 2005, pp. 161-170.

[16] Kanokjaruvijit K, Martinez-Botas RF, "Parametric effects on heat transfer of impingement on dimpled surface," *Journal of Turbimachinery*, Vol. 127, No. 2, 2005, pp. 287-296.

[17] Kanokjaruvijit K, Martinez-Botas RF, "Heat transfer and pressure investigation of dimple impingement," *Journal of Turbomachinery*, Vol. 130, No. 1, 2008, 011003.

[18] Kanokjaruvijit K, Martinez-Botas RF, "Heat transfer correlations of perpendicularly impinging jets on a hemispherical-dimpled surface," *International Journal of Heat and Mass Transfer*, Vol. 53, No. 15-16, 2010, pp. 3045-3056.

[19] Xing Y, Weigand B, "Experimental investigation of impingement heat transfer on a flat and dimpled plate with different crossflow schemes," *International Journal of Heat and Mass Transfer*, Vol. 53, No. 19-20, 2010, pp. 3874-3886.

[20] Kim SM, Kim KY, "Evaluation of cooling performance of impinging jet array over various dimpled surfaces," *Heat and Mass Transfer*, Vol. 52, No. 4, 2016, pp. 845-854.

[21] Xie Y, Li P, Lan J, Zhang D, "Flow and heat transfer characteristics of single jet impinging on dimpled surface," *Journal of Heat Transfer*, Vol. 135, No. 5, 2013, 052201.

[22] Luo L, Wang C, Wang L, Sunden BA, Wang S, "A numerical investigation of dimple effects on internal heat transfer enhancement of a double wall cooling structure with jet impingement," *International Journal of Numerical Methods for Heat and Fluid Flow*, Vol. 26, No. 7, 2016, pp. 2175-2197.

[23] Schukin AV, Kozlov AP, Agachev RS, "Study and application of hemispheric cavities for surface heat transfer augmentation," Proceedings of International Gas Turbine and Aeroengine Congress and Exposition, 2015.

[24] Chang SW, Jan YJ, Chang SF, "Heat transfer of impinging jet-array over convex-dimpled surface," *International Journal of Heat and Mass Transfer*, Vol. 49, 2006, pp. 3045-3059.

[25] Chang SW, Liou HF, "Heat transfer of impinging jet-array onto concave- and convex-dimpled surfaces with effusion," *International Journal of Heat and Mass Transfer*, Vol. 52, 2009, pp. 4484-4499.

[26] Huang X, Yang W, Ming T, Shen W, Yu X, "Heat transfer enhancement on a microchannel heat sink

with impinging jets and dimples," *International Journal of Heat and Mass Transfer*, Vol. 112, 2017, pp. 113-124.

[27] Singh P, Ekkad SV, "Detailed heat transfer measurements of jet impingement on dimpled target surface under rotation," *Journal of Thermal Science and Engineering Applications*, Vol. 10, No. 3, 2018, 031006.

[28] Vinze R, Khade A, Kuntikana P, Ravitej M, Suresh B, Kesavan V, Prabhu S, "Effect of dimple pitch and depth on jet impingement heat transfer over dimpled surface impinged by multiple jets," *International Journal of Thermal Sciences*, Vol. 145, 2019, 105974.

[29] Menter FR, "Two-equation eddy-viscosity turbulence models for engineering applications," *AIAA Journal*, Vol. 32, 1994, pp. 1598-1605.

[30] Jing Q, Zhang D, Xie Y, "Numerical investigations of impingement cooling performance on flat and non-flat targets with dimple/protrusion and triangular rib," *International Journal of Heat and Mass Transfer*, Vol. 126, 2018, pp. 169-190.